Plant Soil (2013) 362:1–23
DOI 10.1007/s11104-012-1455-5

MARSCHNER REVIEW

# Application of ground penetrating radar for coarse root detection and quantification: a review

**Li Guo · Jin Chen · Xihong Cui · Bihang Fan · Henry Lin**

Received: 11 July 2012 / Accepted: 5 September 2012 / Published online: 5 October 2012


**Abstract**
*Background and Scope* Because of the crucial role coarse roots (>2 mm diameter) play in plant functions and terrestrial ecosystems, detecting and quantifying the size, architecture, and biomass of coarse roots are important. Traditional excavation methods are labor intensive and destructive, with limited quantification and repeatability of measurements over time. As a nondestructive geophysical tool for delineating buried features in shallow subsurface, ground penetrating radar (GPR) has been applied for coarse root detection since 1999. This article reviews the state-of-knowledge of coarse root detection and quantification using GPR, and discusses its potentials, constraints, possible solutions, and future outlooks. Some useful suggestions are provided that can guide future studies in this field.
*Conclusions* The feasibility and accuracy of coarse root investigation by GPR have been tested in various site conditions (mostly in controlled conditions or within plantations) and for different plant species (mostly tree root systems). Thus far, single coarse root identification and coarse root system mapping have been conducted using GPR, including roots under pavements in urban environment. Coarse root diameter and biomass have been estimated from indexes extracted from root GPR radargrams. Coarse root development can be observed by repeated GPR scanning over time. Successful GPR-based coarse root investigation is site specific, and only under suitable conditions can reliable measurements be accomplished. The best quality of root detection by GPR is achieved in well-drained and electrically-resistive soils (such as sands) under dry conditions. Numerous factors such as local soil conditions, root electromagnetic properties, and GPR antenna frequency can impact the reliability and accuracy of GPR detection and quantification of coarse roots. As GPR design, data processing software, field data collection protocols, and root parameters estimation methods are continuously improved, this noninvasive technique could offer greater potential to study coarse roots.

**Keywords** Ground penetrating radar · Coarse root · Root system · Root detection · Root quantification

**Abbreviations**

| | |
|---|---|
| DC | Direct current |
| EM | Electromagnetic |
| RMSE | Root mean square error |
| GPR | Ground penetrating radar |
| ERT | Electrical resistivity tomography |

Responsible Editor: Philippe Hinsinger.

L. Guo · J. Chen · X. Cui · B. Fan
State Key Laboratory of Earth Surface Processes and Resource Ecology, Beijing Normal University, Beijing 100875, China

H. Lin (✉)
Department of Ecosystem Science and Management, The Pennsylvania State University, University Park, PA 16802, USA
e-mail: henrylin@psu.edu

## Introduction

Because of differences in morphology and function, fine and coarse roots (also known as structural roots or woody roots) are usually distinguished in root studies (Persson 2002). In general, coarse roots are arbitrarily defined as roots with at least 2 mm in diameter (e.g., Millikin and Bledsoe 1999; Resh et al. 2003). The principle functions of coarse roots for a plant include the uptake and transport of soil-based resources such as water and nutrients, the framework upon which fine roots develop and connect, the storage of photosynthate, and the provision of physical support for the shoot system (Deans 1981; Millikin and Bledsoe 1999; Resh et al. 2003; Reubens et al. 2007a; Brassard et al. 2011). These functions set the requirements on the size and the architecture of coarse roots (Persson 2002; Kalliokoski et al. 2008), making coarse roots spatial configuration detection an important objective in coarse root studies.

Coarse roots also play an important ecological role. The turnover of coarse roots can slowly input carbon and nutrients into soils and soil biota, affecting long-term ecosystem productivity and $CO_2$ emission (Resh et al. 2003). In the context of global change, elevated $CO_2$ concentration and temperature combined with rapid and accelerating changes in land use and precipitation pattern are known to have impacts on ecosystem sustainability (Brunner and Godbold 2007). Coarse root biomass, a crucial element of ecosystem carbon budget (Misra et al. 1998; Miller et al. 2006), has been tested to positively correlate with elevated $CO_2$ concentration (Stover et al. 2007). Therefore, accurate quantification of coarse root biomass is critical for predicting the impact of future climate change on global carbon dynamics (Brassard et al. 2011).

However, embedded in the opaque belowground and closely conjoined with adjacent soils, coarse roots are often challenging for quantitative measurements (Čermák et al. 2000). Traditionally, coarse roots are measured through destructive methods (such as excavation, uprooting, soil block, and profile wall technique), which are direct but laborious and time-consuming, thus restricting the manageability of sampling numbers and the repeatability of measurements (Deans 1981; Oliveira et al. 2000; Van Noordwijk et al. 2000; Polomski and Kuhn 2002; Reubens et al. 2007a). In addition, these destructive methods introduce external disturbance to rhizosphere environment and/or destroy root systems if not done appropriately, making long-term repeated measurements inaccurate or impossible (Van Noordwijk et al. 2000; Nadezhdina and Čermák 2003; Reubens et al. 2007b; Danjon and Reubens 2008). Consequently, significant efforts (e.g., Berntson et al. 1995; Hruška et al. 1999; Čermák et al. 2000, 2008; Zenone et al. 2008; Leucci 2010) have been made to develop nondestructive coarse roots analysis methods in recent decades, including labeling methods (e.g., radioisotopes and stable isotopes labeling), sap flow approaches, and geophysical imaging techniques (e.g., electrical resistivity tomography, seismic refraction tomography, and ground penetrating radar). The nondestructive methods allow a continuous and long-term observation of coarse roots with minimum disturbance. Combining large scale nondestructive observations with small scale destructive techniques (which provides validation and calibration for the results from nondestructive observations) shows great potential for coarse roots field monitoring.

Ground penetrating radar (GPR), a nondestructive geophysical technique widely used in locating underground objects (e.g., restrictive soil horizons, stone lines, bedrocks, water tables, buried artifacts, pipes, and cables) (Conyers and Goodman 1997; Daniels 1996; Jol 2009) has been tested for coarse root detection, coarse root mapping, and coarse root diameter and biomass estimation since 1999 (Hruška et al. 1999; Butnor et al. 2001). However, conflicting conclusions have been reported in different studies (e.g., Barton and Montagu 2004; Dannoura et al. 2008; Hirano et al. 2009; Cui et al. 2011). In addition, some limitations of GPR detection of coarse roots have also been recognized (Butnor et al. 2001; Hirano et al. 2009). Applying GPR for coarse root quantification is still in its infancy, but has shown interesting potential (Bassuk et al. 2011) in determining coarse root related parameters (Stover et al. 2007), especially when various limiting factors have been evaluated and avoided (Dannoura et al. 2008). Hence, a comprehensive review of published works on coarse root detection and quantification by GPR is valuable for establishing standard protocols with optimal choices for using this technique under different conditions.

The objectives of this paper are two-fold: (1) to review the state-of-knowledge of coarse root measurement using GPR, including major GPR post-processing methods and main factors influencing the reliability and accuracy of the GPR detection of coarse

roots; and (2) to discuss current challenges and possible solutions of coarse root detection and quantification using GPR and to provide some future outlooks. The paper is organized as follows: After reviewing GPR principle and GPR signal processing, we discuss various GPR applications to coarse root detection and quantification as well as limiting factors that influence the quality of GPR-based coarse root investigation. Finally, we provide some future outlooks to guide future efforts in this area.

## GPR principle

Ground penetrating radar is an electromagnetic (EM) technique used to detect changes in physical properties (especially the relative dielectric permittivity, which is a general measurement of how well EM energy is transmitted through a medium) within the shallow subsurface (Daniels 1996; Conyers and Goodman 1997). A standard GPR system consists of three basic components: the control unit (including pulse generator, computer, and associated software), the antennas (including paired transmitting and receiving antennas), and the display unit (Conyers 2004) (Fig. 1a). During GPR detection, high frequency EM energy (composed of conjoined oscillating electrical and magnetic fields) generated by transmitting antenna propagates into the ground as waves.

When radar waves pass across interfaces between media with different electrical or magnetic properties, reflections are generated (Fig. 1a) (al Hagrey 2007). Then a portion of energy will be reflected back to the surface and recorded by the receiving antenna, while the remainder continues to propagate deeper until it is attenuated thoroughly (Barton and Montagu 2004). After being sampled and digitized by control unit, reflected waves are combined into a reflection trace (also named A-scan), recording the two-way travel time (i.e., the time elapsed between emission and detection of the reflected signal) on the vertical axis and the amplitudes of the return signals as well as their polarities along the horizontal axis (Fig. 1b) (Hruška et al. 1999; Barton and Montagu 2004).

The depth of an object or interface inducing radar reflections can be resolved if the propagation velocity ($V$) is known (Daniels 1996):

$$D = \frac{V \times t}{2}, \tag{1}$$

where $D$ is the depth and $t$ is the two-way travel time. Wave velocity can be obtained from the following equation (Lorenzo et al. 2010):

$$V = \frac{1}{\sqrt{\frac{\mu\varepsilon}{2}\left(\sqrt{1+\left(\frac{\sigma}{\omega\varepsilon}\right)^2}+1\right)}}, \tag{2}$$

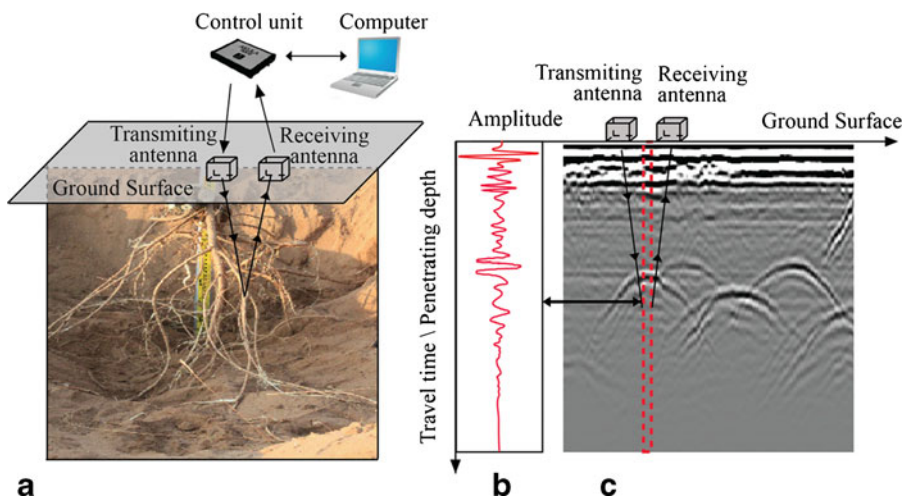


**Fig. 1** Schematic illustration of GPR detection of *Caragana microphylla* roots in a sandy area in the Inner Mongolia, China: **a** High frequency electromagnetic pulses emitted from a transmitting antenna reflect off the boundary between soils and roots and then received by a receiving antenna. Time and signal strength are recorded by the control unit; **b** A reflected waveform (A-scan) of GPR radargram recording the two-way travel time (i.e., the penetrating depth) on the vertical axis and amplitudes of the return signals along the horizontal axis; **c** A raw GPR radargram (B-scan) corresponding to (**a**), with hyperbolic shaped reflections representing root reflectors

where $\mu$ is the magnetic permeability, $\sigma$ is the electrical conductivity, $\varepsilon$ is the dielectric permittivity, and $\omega$ is the angular frequency (i.e., $\omega=2\pi f$, where $f$ is frequency) of the emitted pulse. For low conductive and nonmagnetic materials (i.e., $\sigma << \omega\varepsilon$ and $\mu_r=1$, where $\mu_r$ is the relative magnetic permeability), propagation velocity can be estimated by the formula (al Hagrey 2007):

$$V = \frac{1}{\sqrt{\mu\varepsilon}} = \frac{c}{\sqrt{\varepsilon_r}}, \tag{3}$$

where $c$ is the speed of light in vacuum (0.2998 m per nanosecond) and $\varepsilon_r$ is the relative dielectric permittivity.

The strength of reflections at an interface between two materials depends on the reflection coefficient $R$ (Conyers 2004; al Hagrey 2007):

$$R = \frac{\sqrt{\varepsilon_{r1}} - \sqrt{\varepsilon_{r2}}}{\sqrt{\varepsilon_{r1}} + \sqrt{\varepsilon_{r2}}} = \frac{V_2 - V_1}{V_1 + V_2}, \tag{4}$$

where $\varepsilon_{r1}$ is the relative dielectric permittivity of the overlying material, $\varepsilon_{r2}$ is the relative dielectric permittivity of the underlying material, $V_1$ is the propagation velocity in the overlying material, and $V_2$ is the propagation velocity in the underlying material. Apparently, it is the relative dielectric permittivity contrast between the neighboring media that determines the strength of reflected energy (Conyers and Goodman 1997). Higher water content in roots than in soil matrix can provide the necessary permittivity contrast, making root detection by GPR possible (Wielopolski et al. 2000; Cui et al. 2011).

While dragging a radar unit along a detection transect, EM pulses are generated at a certain interval of time or distance and a cross-section of reflected signals can be recorded (Fig. 1c). The traces can be integrated into a radargram (also called B-scan) that portray the nature of buried materials on a vertical scale with two-way travel time (or approximate depth) on the vertical axis and surface location on the horizontal axis (Fig. 1c) (Butnor et al. 2001; Barton and Montagu 2004).

Ground penetrating radar transmitting antenna generates energy in a beam that travels downward into the ground in an elliptical cone (Fig. 2a) (Annan and Cosway 1994; Conyers 2004). With increasing propagation depth, the radius of cone also expands, resulting in a larger footprint scanned beneath the antenna (Conyers 2004). The footprint area can be approximated by the formula (Conyers and Goodman 1997):

$$A = \frac{\lambda}{4} + \frac{D}{\sqrt{\varepsilon_r + 1}}, \tag{5}$$

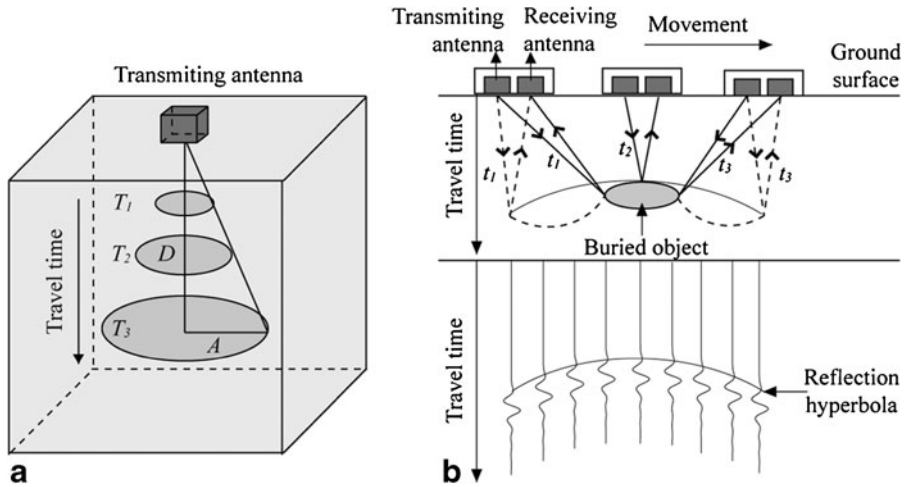


**Fig. 2** Schematic illustration of the conical radiating pattern of GPR waves and the generation of a reflection hyperbola: **a** Spreading footprint of wave from antenna with increasing traveling time. $T_1$, $T_2$ and $T_3$ are the increased travel times, $D$ is the traveling depth, and $A$ is the long dimension radius of footprint. **b** Upper: the conical radiation of radar beam allows the radar signal to be reflected by a buried object before and after antennae are directly above it. The two-way travel time ($t_1$, $t_2$ and $t_3$) is recorded and plotted in depth directly below the antennae. Lower: different A-scans along the antennae moving direction showing a reflection hyperbola

where $A$ is the long dimension radius of footprint, $\lambda$ is the center frequency wavelength of radar energy, $D$ is the depth from ground surface to reflection surface, $\varepsilon_r$ is the average relative dielectric permittivity of scanned material from ground surface to the depth of reflector ($D$). The GPR resolution, the capacity to discriminate between two closely-spaced targets as well as the minimum size detectable, is negatively correlated with footprint area (Butnor et al. 2001). The minimum detectable size of an object is smaller than the minimum space between adjacent objects that can be discriminated. For a 900 MHz GPR system, the diameter of the smallest detectable root is 1.9 cm, while the detectable smallest interval between closely-located roots is between 10 ~ 20 cm (Hirano et al. 2009) (Table 1). Generally, the cross-sectional area of the target to be delineated should approximate the size of footprint area. Thus, according to Eq. 5, GPR detection resolution depends on the antenna frequency, EM properties of medium, and the penetrating depth (see Fig. 3.19 in Conyers 2004). Table 1 summarizes the resolution of coarse root detection using GPR with different antenna center frequencies based on published works. The general range of the minimum detectable root size varied from 1 to 4 cm, 1 to 2.5 cm, and 0.25 to 0.5 cm for antenna center frequencies between 400 and 500 MHz, 800 and 1,000 MHz, and 1,500 and 2,000 MHz, respectively.

Because of the conical radiating pattern of GPR waves, radar energy from small features (such as the cross section of roots) will therefore be reflected before and after the antenna is dragged directly above them (Butnor et al. 2001; Conyers 2004). As the antenna moves closer to the buried object, the recorded two-way travel time decreases until the antenna is directly over it. When the antenna moves away from the object, the same phenomenon is repeated in reverse, generating a reflection hyperbola with its apex denoting the actual location of buried object (Fig. 2b) (Conyers 2004). However, clear reflection hyperbolas are only generated from small individual objects or linear objects that are crossed at right angles to the antenna's moving direction (Butnor et al. 2001; Barton and Montagu 2004). When the crossed angles are less than 45°, linear buried object generate elongate linear reflections on GPR radargrams (Butnor et al. 2001; Barton and Montagu 2004).

When penetrating through media, radar energy decays exponentially with propagation time (Neto and de Medeiros 2006):

$$A(f,t) \propto \exp(-V\alpha t), \tag{6}$$

where $A(f, t)$ is the value of the amplitude in the two-way travel time $t$ with the antenna center frequency $f$, $V$ is the wave velocity, and $\alpha$ is the attenuation coefficient (which is frequency dependent). Thus, as transmitted energy penetrates more deeply into the ground, less is available for reflection from successive interfaces. As a result, GPR is designed primarily to investigate shallow subsurface and targets buried within shallow subsurface, where sufficient radar energy can be maintained to be reflected back to the receiving antenna (Conyers 2004).

Although B-scan is the primary product of GPR detection, B-scan diagram is difficult to provide lifelike renderings of a survey site. Fortunately, recent advancements in GPR data processing and visualization software have facilitated the creation of 3D pseudo-images (also called C-scan) of the subsurface by interpolating multiple 2D radargrams (Jol 2009). Through introducing color as the fourth dimension, different interesting ways of portraying buried objects detected by GPR are possible. This is further discussed in Section 4.

## GPR signal processing

Signal processing is a critical step in appropriate interpretation of GPR data. Because of wide-ranging possibilities of GPR signal processing, only those methods employed in GPR root detection are reviewed here. Signal processing is necessary both during and after GPR scanning. During scanning, signal processing methods and the corresponding parameters should be optimized according to specific conditions of an investigation site. Hence, a standard protocol for signal processing during scanning may be difficult to establish because of diverse site conditions. Among those studies on the detection of roots using GPR, only Wielopolski et al. (2000) and Butnor et al. (2003) have particularly described their signal processing settings during scanning, including vertical digital filters (low pass filter and high pass filter) and horizontal smoothing. These filters help improve the signal to noise ratio by reducing low frequency (appears as horizontal bands of noise) and high frequency (appears as spikes

**Table 1** The maximum effective detection depth and resolution of GPR systems with different radar center frequencies used for root detection in various soil types

| Antenna center frequency (MHz) | Soil Type | Soil texture[a] | | Soil drainage condition | Site condition and plant species | GPR scanning length (m) | Maximum detection depth (m) | Resolution (cm)[b] | Reference |
|---|---|---|---|---|---|---|---|---|---|
| | | Sand (%) | Clay and Silt (%) | | | | | | |
| 250 | - | - | - | Poor | Natural riparian forest, Mopani tree (*Colophospermum mopane*) | 96.0 | 4.00 | - | Schoor and Colvin 2009 |
| 400 | Gergeville soil | 65 | 35 | Well | Plantation, Loblolly pine (*Pinus taeda*) | - | 1.00 | 3.7 | Butnor et al. 2001 |
| 400 | Lynchburg soil | 70 | 30 | Poor | Plantation with debris and litter on surface, Loblolly pine (*Pinus taeda*) | - | 1.30 | - | Butnor et al. 2001 |
| 400 | Wakulla soil | 85 ~ 92 | 8 ~ 15 | Well | Plantation, Loblolly pine (*Pinus taeda*) | 6.6 | 1.00 | - | Butnor et al. 2001 |
| 450 | Loamy deluvium soil | 30 ~ 60 | 40 ~ 70 | Well | Plantation, Oak (*Quercus petraea*) | 156.0 | 2.20 | 3.0 ~ 4.0 | Hruška et al. 1999 |
| 450 | Loess-Clay soil | < 50* | > 50* | Poor | Urban setting with pavement and lawn on surface, Maple (*Acer campestre*) | 276.0 | 2.00 | 2.0 ~ 3.0 | Čermák et al. 2000 |
| 450 | Loess-Clay soil | < 50* | > 50* | Well | Urban setting with lawn on surface, Pine (*Pinus nigra*) and Mountain ash (*Sorbus intermedia*) | 301.0 | 2.50 | 2.0 | Stokes et al. 2002 |
| 500 | River sand | 100* | 0* | Well | Controlled in field with clear surface, Eucalyptus (*Eucalyptus sp.*) | 52.0 | - | 1.0, 25.0† | Barton and Montagu 2004 |
| 800 | River sand | 100* | 0* | Well | Controlled in field with clear surface, Eucalyptus (*Eucalyptus sp.*) | 52.0 | 1.55 | < 1.0 | Barton and Montagu 2004 |
| 900 | Loamy sand | 92 | 7 | - | Controlled in field with clear surface, Peach (*Prunus persica*) | 110.0 | 1.14 | 2.5 | Cox et al. 2005 |
| 900 | Loamy sand | 85 | 15 | - | Orchard, Peach (*Prunus persica*) | 432.0 | - | 1.2 | Cox et al. 2005 |
| 900 | Sand | 100* | 0* | Poor | Controlled in field with clear surface, Conifer (*Cryptomeria japonica*) | 49.0 | - | 1.1 | Dannoura et al. 2008 |
| 900 | Sand | 100* | 0* | Well | Controlled in field with clear surface, Conifer (*Cryptomeria japonica*) | 77.0 | 0.80 | 1.9, 10.0 ~ 20.0† | Hirano et al. 2009 |
| 1000 | River sand | 100* | 0* | Well | Controlled in field with clear surface, Eucalyptus (*Eucalyptus sp.*) | 52.0 | 1.55 | < 1.0 | Barton and Montagu 2004 |
| 1500 | Sand | 100* | 0* | Well | Controlled in lab with clear surface, a kind of tree | - | - | 0.25 | Wielopolski et al. 2000 |
| 1500 | Lakeland soil | 90 | 10 | Well | Plantation with clear surface, Cottonwood (*Populus deltoides*) | 3.6 | 0.45 | 0.6 | Butnor et al. 2001 |
| 1500 | Lakeland soil | 90 | 10 | Well | Controlled in field with clear surface, Cottonwood (*Populus deltoides*) | - | - | 0.5 | Butnor et al. 2001 |
| 1500 | Wakulla soil | 85 ~ 92 | 8 ~ 15 | Well | Plantation, Loblolly pine (*Pinus taeda*) | 6.6 | 0.50 | 0.5 | Butnor et al. 2001 |
| 1500 | Wakulla soil | 85 ~ 92 | 8 ~ 15 | Well | Controlled in field with clear surface, Loblolly pine (*Pinus taeda*) | - | - | 0.5 | Butnor et al. 2001 |
| 1500 | Lynchburg soil | 70 | 30 | Poor | Plantation with debris and litter on surface, Loblolly pine (*Pinus taeda*) | - | 0.35 | - | Butnor et al. 2001 |

**Table 1** (continued)

| Antenna center frequency (MHz) | Soil Type | Soil texture[a] | | Soil drainage condition | Site condition and plant species | GPR scanning length (m) | Maximum detection depth (m) | Resolution (cm)[b] | Reference |
|---|---|---|---|---|---|---|---|---|---|
| | | Sand (%) | Clay and Silt (%) | | | | | | |
| 1500 | Gergeville soil | 65 | 35 | Well | Plantation, Loblolly pine (*Pinus taeda*) | - | 0.60 | - | Butnor et al. 2001 |
| 1500 | Troup and Lucy soil | > 70* | < 30* | Well | Plantation with litter on surface, Loblolly pine (*Pinus taeda*) | 21.6 | 0.50 | 0.5 | Butnor et al. 2003 |
| 1500 | Sandy Pomello soil | > 90* | < 10* | Well | Plantation, Scrub oak (*Quercus sp.*) | 4.5 | 0.60 | 0.5 | Stover et al. 2007 |
| 2000 | Sand | 95 | 5 | Well | Controlled in field with clear surface, Elm (*Ulmus pumila*) | 50.4 | 0.80 | 0.5 | Cui et al. 2011 |

[a] Refers to the soil texture reported by each study. Those labeled with * are speculated values according to the corresponding soil types

[b] Refers to the minimum detectable root size. The two numbers labeled with † are the minimum detectable interval between closely located roots

or "snow") noise generated by antenna/ground interactions, system noise, or from nearby radio transmitters and other EM frequency interference.

Different from optical image, raw GPR radargrams can hardly provide sufficient geometrical information of buried targets. Furthermore, GPR radargrams are always contaminated by extraneous reflections and clutter reflections. Consequently, raw GPR radargrams must be cleaned up and adjusted prior to interpretation. The general objective of signal post-processing is either to prepare an image that can readily be interpreted or to classify the target return with respect to a known test procedure (Daniels 2004). For root detection, Butnor et al. (2003) first provided an advanced data post-processing flow protocol that was accepted and modified in other studies. After being improved by Barton and Montagu (2004) and Stover et al. (2007), a standard GPR data post-processing protocol for the detection and quantification of roots has been gradually established. The post-processing steps used in various studies are summarized in Table 2. Generally, a standard GPR data post-processing protocol should include radargram standardization, noise reduction, signal amplification, migration and Hilbert transformation. Each of these steps is briefly summarized below.

Radargram standardization is used to correct the vertical and horizontal scales on the radargrams. During this process, the offset in time between zero in the time window and the first break (i.e., the time needed for the first reflection from ground surface) among each trace can be compensated by removal of the direct current (DC) offset and DC drift (e.g., Barton and Montagu 2004) or by least-square fitting analysis of the first break (e.g., Cui et al. 2011). If GPR data are collected over uneven ground or without a survey wheel, the horizontal scale of the radargram is not uniform. With the help of impressed markers on GPR radargram at known space or distance intervals, the horizontal distance could be normalized or terrain-corrected (e.g., Butnor et al. 2003; Cox et al. 2005).

Background noise on GPR radargrams include horizontal bandings caused by antenna/ground interactions or nearby radio interference, multiple reflections produced by GPR signal reflecting between subsurface layers, and high frequency spike events. Noise reduction is performed to these unwanted reflections. Background removal filters (also called Finite Impulse Response filters) can be applied to remove parallel bands of low

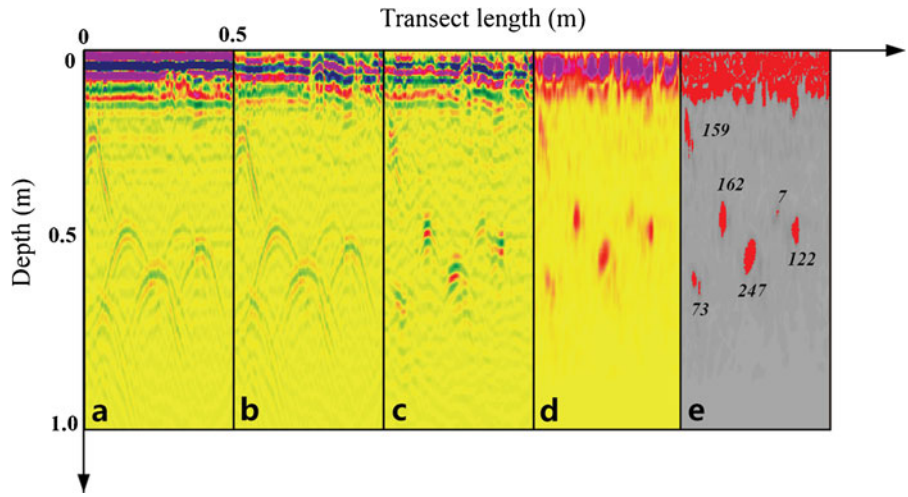


**Fig. 3** An example of GPR radargrams collected from a shrub (*Caragana microphylla*) in a sandy area in the Inner Mongolia, China, showing the capacity of GPR for detecting two pieces of roots and the effect of post-processing of GPR image: **a** Raw data from an IDS GPR system with 900 MHz antenna with the hyperbolic reflections representing the root reflectors; **b** Same radargram processed in Reflex-Win 5.0 software (Sandmeier Scientific Software, Germany) with DC drift removal, background removal and band pass filter (both high-pass and low-pass filter) used to eliminate low frequency noises and high frequency noises; **c** *Kirchoff* migration used to trace hyperbola reflections back to their sources; **d** *Hilbert* transformation used to express the magnitude of signals to elucidate subtle objects and reduce multiple reflections; **e** Radargram was converted to 8-bit gray scale image. Highlight areas indicate the pixels within threshold range (intensity from 60 to 255) extracted with Sigma Scan software (Systat Software Inc., USA). Numbers listed above root radar signals are the sum of pixels within threshold range of each root radar signal. The scale used for plotting the data is identical for each subfigure

frequency noise (e.g., Butnor et al. 2003; Stover et al. 2007). Noise caused by low-frequency interference can also be eliminated by high-pass filter (e.g., Cui et al. 2011). High frequency noise can be suppressed by gradient filter (e.g., Barton and Montagu 2004) or stacking several traces together.

From GPR theory, the strength of radar signal deteriorates exponentially with travel time (see Eq. 6). Time varying gain adjustments can be used to compensate for the energy loss caused by medium attenuation, scattering losses, and dissipation. Barton and Montagu (2004) applied a combination of linear and exponential gain to radargrams to intensify the visibility of hyperbolas. In other studies (e.g., Butnor et al. 2003; Cox et al. 2005), range gains were set and adjusted before a radar survey was conducted. However, the noise strength on GPR radargrams would be increased simultaneously.

Raw GPR radargrams portray a distorted image of subsurface stratigraphy and buried features. Point reflectors, such as roots (crossed with antenna orthogonally to their long axes), generate hyperbola reflections, making the delineation of buried targets from GPR radargrams indirect. Distortions can be corrected by the application of migration, which traces hyperbola reflections back to their sources and removes the "arms' or "tails" of the hyperbolas. *Kirchoff* migration is a common migration method used in the detection of root by GPR. This method first calculates the incidence angle and the distance to a buried reflector. Then the position of target reflector is corrected by collapsing hyperbola arm to its apex (Conyers 2004). Unsupervised maximum-convexity migration can be applied as an alternative method (Barton and Montagu 2004). This method assumes a semi-hyperbolic maximum convexity function and sums the value of each separate A-scan at the point at which it intersects the semi-hyperbolic focus over the ensemble data set. All in-phase energy adds in phase, whereas noncoherent energy is usually out of phase and tends to be zero (Daniels 1996). For both unsupervised maximum-convexity migration and *Kirchoff* migration, knowledge of GPR wave velocity is required for proper interpretations. The wave velocity can be estimated by soil $\varepsilon_r$ based on Eq. 3 (e.g., Čermák et al. 2000) or measured by burying a metallic object at a known depth (e.g., Butnor et al. 2003) or determined by using the characteristic hyperbolic shape of reflection from a point source (e.g., Barton and Montagu 2004).

Different from migration, the *Hilbert* transformation expresses the relationship between the magnitude and the phase of radar signal allowing the phase of the signal to be reconstructed from its amplitude instead of its geometry, thus allowing subtle properties and objects to be elucidated and reducing multiple reflections (Oppenheim and Schafer 1975). The hyperbola reflections generated by roots can also be decomposed by this method. In some studies, migration was omitted due to the application of *Hilbert* transformation (e.g., Butnor et al. 2003; Samuelson et al. 2008).

Although the specific algorithms used in each post-processing step varied among different studies, the primary steps are converged as summarized in Table 2. The effect of major signal processing procedures on GPR radargram is illustrated in Fig. 3. Overall, advanced GPR post-processing techniques have significantly improved the quality of radargrams and benefited the quantitative measurements of coarse roots as described in the following section.

## Applying GPR for coarse root detection and quantification

Although roots have commonly been identified in soil GPR images (Cammarano and Piro 1997; Papamarinopoulos et al. 1997), they have been considered as unwanted noise that hinder the interpretation of GPR radargrams (Doolittle and Miller 1991). Hruška et al. (1999) first applied GPR technique for coarse root detection and claimed that GPR was an appropriate tool for coarse root mapping. The major interests of using GPR to detect coarse root thus far include: 1) coarse root mapping (e.g., Hruška et al. 1999; Čermák et al. 2000; Wielopolski et al. 2000; Stokes et al. 2002; Cox et al. 2005; Samuelson et al. 2008; Zenone et al. 2008; Schoor and Colvin 2009; Leucci 2010; Bassuk et al. 2011); and 2) coarse root biomass and diameter estimation (e.g., Butnor et al. 2001, 2003; Barton and Montagu 2004; Butnor et al. 2005; Cox et al. 2005; Stover et al. 2007; Butnor et al. 2008; Samuelson et al. 2008; Dannoura et al. 2008; Hirano et al. 2009; Lorenzo et al. 2010; Cui et al. 2011). In what follows, each of the applications is comprehensively reviewed.

### Coarse root mapping

Coarse root mapping can be divided into 3D root system architecture reconstruction and 2D/3D root zone mapping. At the beginning stage of using GPR for root investigation, most efforts were made to test the applicability of GPR for imaging root 3D architecture (e.g., Hruška et al. 1999; Čermák et al. 2000; Stokes et al. 2002). In these studies, a GPR system

**Table 2** Various post-processing routines used in different studies of roots using GPR

| Studies | Post-processing steps | | | | |
|---|---|---|---|---|---|
| | Radargrams standardization | Noise reduction | Signal amplification | Migration | Hilbert Transformation |
| Hruška et al. 1999 | | √ | √ | √ | |
| Wielopolski et al. 2000 | √ | √ | | √ | √ |
| Butnor et al. 2001 | √ | √ | | | |
| Butnor et al. 2003 | √ | √ | | √ | √ |
| Barton and Montagu 2004 | √ | √ | √ | √ | |
| Cox et al. 2005 | √ | √ | | √ | |
| Stover et al. 2007 | √ | √ | | √ | √ |
| Dannoura et al. 2008 | √ | √ | | √ | √ |
| Butnor et al. 2008 | √ | √ | | √ | √ |
| Samuelson et al. 2008 | √ | √ | | | √ |
| Hirano et al. 2009 | √ | √ | | √ | √ |
| Leucci et al. 2010 | | √ | | √ | |
| Cui et al. 2011 | √ | √ | | √ | |

with center frequency of 450 MHz was employed to map coarse roots of four different tree species in various soil conditions (even in urban environments, see Table 1). After data post-processing steps (including signal amplification and migration), 3D views of the coarse root system (Fig. 4) were redrawn manually based on the GPR radargram. Then the root systems were digitized for determining coarse root length and coarse root area density at different depths. However, no specific information was provided in these studies regarding how the root map was redrawn from the GPR radargram. It seemed that root locations and diameters were first estimated on each radargram and roots between neighboring radargrams were subjectively linked to create a root 3D map.

There are several advantages of coarse root mapping using GPR over other methods, including 1) scanning root systems noninvasively and efficiently; and 2) allowing repeated and long-term observation of root distribution and development beneath various landscapes (Hruška et al. 1999). However, when coarse roots were manually redrawn according to GPR radargrams and compared with actual field observations obtained through excavation and photography, only limited similarities were found in coarse root architectures, especially in vertical views (e.g., see Figs. 3 and 4 in Stokes et al. 2002). This was caused by the fact that GPR could not identify objects running parallel to EM pulses propagating direction, and their data analysis methods were unable to differentiate roots from different plants. Moreover, since the final root maps were redrawn arbitrarily from GPR radargrams according to operator's personal experience, bias may be introduced during root diameter estimation and branching pattern conjecture. Therefore, it is challenging to apply such method to reconstruct 3D coarse root system architecture. Recently, Zenone et al. (2008) tested the feasibility of using GPR for 3D coarse root system architecture reconstruction. In this study, a GPR system with center frequency of 1,500 MHz was employed to scan root systems in situ. Then the investigated root systems

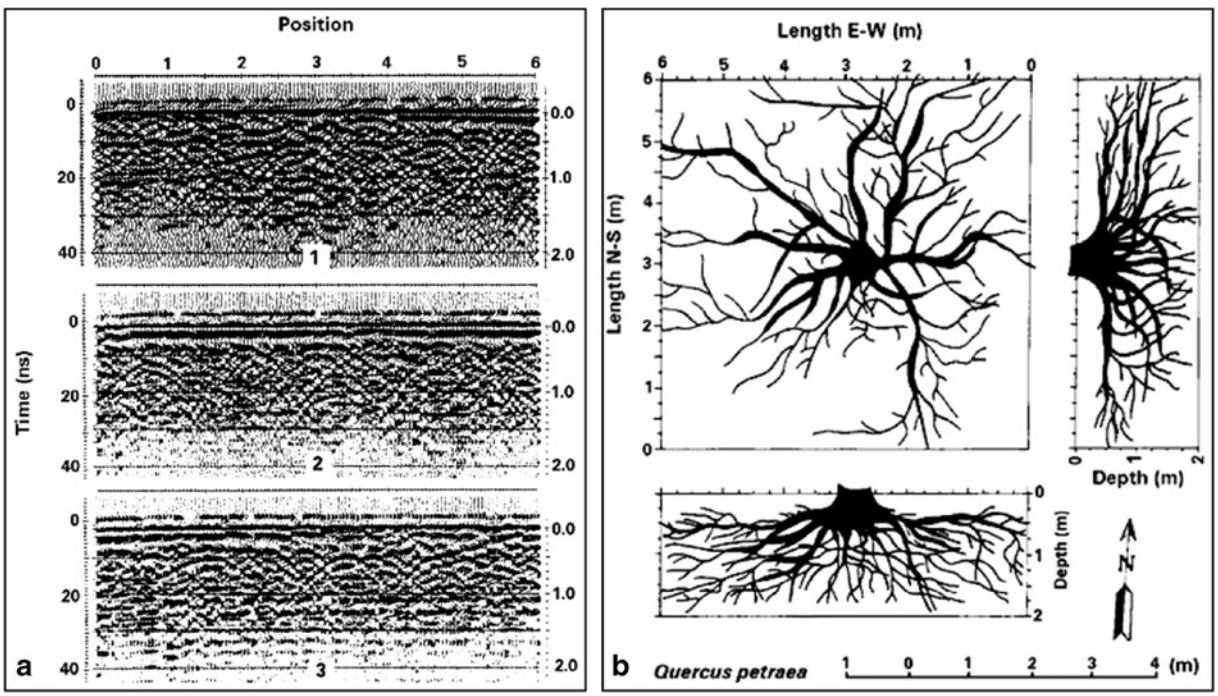


**Fig. 4** Mapping root system using GPR: **a** In situ GPR radargrams with numerous oak (*Quercus petraea*) root indications. Root locations and diameters on each radargram were estimated. Through linking root reflectors on the neighboring GPR radargrams, the orientation and length of each single root were obtained, and then different views of the root system were redrawn manually; **b** Ground plan, front, and side views of the root system. The maximum rooting depth, root branching pattern, and root spatial distribution pattern were extracted based on the images shown in (**a**) (from Hruška et al. 1999, Figs. 2 and 4; reprint with permission from Oxford University Press)

were entirely excavated by air-spade and pulled out by a digger. A laser measurement system was applied to scan the whole excavated root systems and the 3D root system architectures were reconstructed. The 3D rendering of migrated GPR scans was compared with the laser-scan point cloud (Fig. 5). However, no real correspondence between GPR-based coarse root architecture and the excavated root system was found in this study. Although the authors of this study stated that root system architecture might have been altered during excavation, which could partially explain the mismatching between GPR detection results and ground truthing, the fact that using GPR for 3D coarse root system architecture reconstruction remains questionable should be further investigated.

While it is debatable in applying GPR for coarse root system 3D branching architecture imaging, the feasibility of using GPR for coarse root detection and single coarse root 3D imaging have been proved. Bassuk et al. (2011) used a GPR system with a 900 MHz antenna mounted on a root-scanning cart to identify coarse roots buried under concrete. Although the clustering of fine roots was not detectable individually and resulted in some differences between root counts from GPR

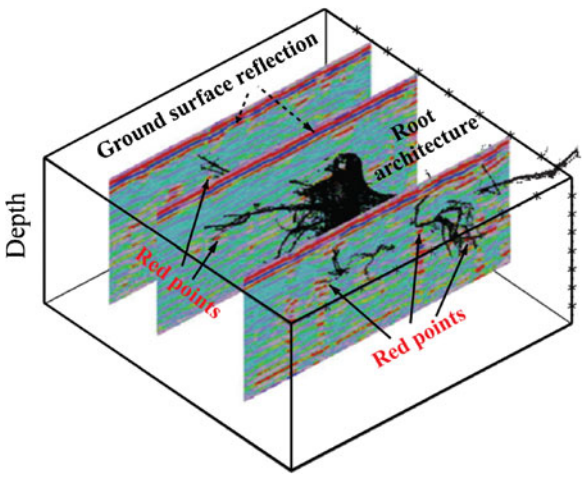


**Fig. 5** A comparison between actual 3D coarse root architecture of *Pinus sp.* and sections of GPR scans. The horizontal strong bands on the top of each radargram indicated by the dashed arrows were ground surface reflections. The red points on GPR radargrams represent coarse root positions. Root architecture was obtained through laser scanning after root system was excavated by an air spade and a digger. Only limited correspondence between red points (indicating GPR detected roots) and excavated roots can be observed (adapted from Zenone et al. 2008, Fig. 6; reprint with permission from CSIRO Publishing)

scanning and those from excavation, this study showed that GPR reliably predicted coarse root presence. Moreover, Cox et al. (2005) also validated the accuracy of applying GPR for coarse root detection and pointed out that the correspondence between GPR reflector and root relied on the strength and shape of the reflections (stronger reflection amplitude and better-defined hyperbolic shape would lead to a better correspondence). Using a GPR system with center frequency of 1,500 MHz, Wielopolski et al. (2000) successfully obtained 3D images from radar scans of individual "root samples" buried in a sand box (with fresh tree twigs used to simulate roots). With the aid of visualization software, reconstructed 3D images of the "root" samples and their volumes were obtained. They concluded that many aspects of GPR hardware, visualization software, and signal processing methods need to be improved before precise 3D root system images could be reconstructed from radargrams. Due to the difficulty of root 3D architecture reconstruction, some studies (e.g., Lorenzo et al. 2010; Leucci 2010) attempted to apply GPR to resolve root-zone (i.e., the region of soil located in and around the root system) in 2D/3D rather than accurately locate single coarse root. In these studies, GPR was used to scan root systems in a grid (consisting of different parallel lines in both x and y directions). On each B-scan radargram, the probable 2D extension of root zone could be delineated (e.g., see Fig. 15 in Leucci 2010). Certain interpolation method (e.g., inverse distance or kriging) was applied to spatially interpolate processed GPR data into areas between transect lines. Then time slices parallel to the ground surface were generated with amplitude slice-mapping program by averaging the amplitude (or the square amplitude) of the radar signal within a time interval (Leucci 2010). Finally data are gridded on a regular mesh to delineate the root zone area in any depth interval (which could be converted from travel time interval and wave velocity). The 3D horizontal time slice pseudo-images facilitated the characterization of changes in root zones with depth. Unfortunately, these studies failed to evaluate the accuracy of GPR-based root zone mapping, and the quantitative relation between root density and signal strength on time slices was unclear.

## Root related parameters estimation

Besides coarse root mapping, GPR has also been tested for estimating root related parameters such as

coarse root biomass and diameter (which are essential for understanding root functions in ecosystems). Butnor et al. (2001) first used GPR to estimate coarse root biomass and diameter and developed a framework of GPR-based coarse root quantification method. With the aid of advanced GPR data post-processing protocols and new GPR indexes and estimation methods, the accuracy of root related parameters estimations has been improved over the past decade.

The basic steps of GPR-based root quantification include the following:

1) *Data collection*: All coarse root diameter estimation studies were carried out on root samples buried in the ground under controlled conditions (Table 3). Most coarse root biomass estimation studies (with the exception of Cui et al. 2011) were completed on the living root systems in field conditions (Table 4). The specific site conditions and target plant species for each study are listed in Table 1. For controlled experiments, actual coarse root diameters were measured before reburying. For living roots, samples corresponding to locations on radargrams were gathered from soil cores to obtain actual coarse root biomass.
2) *Data post-processing*: Although differences existed between each study, primary data post-processing routines have been gradually established, including GPR radargrams standardization, noise reduction, signal amplification, migration, and *Hilbert* transformation. These steps have been described in Section 3 of this paper.
3) *Index extraction*: GPR indexes used for root related parameters estimation are diverse. Generally, the indexes can be divided into two main groups: a) reflection strength indexes from GPR radargrams (including areas within threshold range, pixels within threshold range, mean pixel intensity, and reflector tally) and b) reflection waveform indexes

**Table 3** A comparison of root diameter estimation using GPR, showing GPR index, target plant species, antenna center frequency, root depth, root size, sample size for correlation analysis, and the Pearson correlation coefficient between GPR index and actual root diameter. The definition of each GPR index is shown in Fig. 6, and *t1*, *t2*, *t3*, $\Delta T$ are different time indices extracted from GPR radargrams

| GPR Index | Plant species | Antenna center frequency (MHz) | Root depth (cm) | Root diameter (cm) | Sample size (n) | Correlation coefficient ($r$) | Reference |
|---|---|---|---|---|---|---|---|
| Areas within threshold range | *Populus deltoides* | 1500 | 20 | 0.5 ~ 6.5 | 9 | 0.46 | Butnor et al. 2001 |
| | *Pinus taeda* | 1500 | 15 | 0.5 ~ 4.5 | 14 | 0.81 | Butnor et al. 2001 |
| | | | 30 | 0.5 ~ 5.0 | 14 | 0.55 | Butnor et al. 2001 |
| Mean pixel intensity | *Prunus persica* | 900 | 11 ~ 114 | 2.5 ~ 8.2 | 24 | −0.52, −0.63[a] | Cox et al. 2005 |
| Pixels within the threshold range | *Cryptomeria japonica* | 900 | 30 | 1.1 ~ 5.2 | 20 | 0.83 | Dannoura et al. 2008 |
| | *C. japonica* | 900 | 30 ~ 80 | 1.9 ~ 7.8 | 30 | 0.75 | Hirano et al. 2009 |
| Amplitude of max reflected wave | *C. japonica* | 900 | 30 | 1.1 ~ 5.2 | 20 | 0.64, 0.76[b] | Dannoura et al. 2008 |
| | *C. japonica* | 900 | 30 ~ 80 | 1.9 ~ 7.8 | 30 | 0.65 | Hirano et al. 2009 |
| High amplitude area | *C. japonica* | 900 | 30 | 1.1 ~ 5.2 | 20 | 0.76, 0.81[b] | Dannoura et al. 2008 |
| | *C. japonica* | 900 | 30 ~ 80 | 1.9 ~ 7.8 | 30 | 0.77 | Hirano et al. 2009 |
| *t1, t2, t3* | *Eucalyptus sp.* | 500 | 15 ~ 155 | 1.0 ~ 8.0 | 34 | 0.94 | Barton and Montagu 2004 |
| *t1* | *C. japonica* | 900 | 30 | 1.1 ~ 5.2 | 20 | 0.50 | Dannoura et al. 2008 |
| *t2* | *C. japonica* | 900 | 30 | 1.1 ~ 5.2 | 20 | 0.77 | Dannoura et al. 2008 |
| *t3* | *C. japonica* | 900 | 30 ~ 80 | 1.9 ~ 7.8 | 30 | 0.31 | Hirano et al. 2009 |
| $\Delta T$ | *Ulmus pumila* | 2000 | 10 ~ 80 | 0.5 ~ 3.5 | 30 | 0.93 | Cui et al. 2011 |

[a] Higher amplitude signals correspond to lower values of pixel intensity, leading to the negative correlation between mean pixel intensity and coarse root diameters. A stronger correlation ($r$=−0.63) was obtained between root depth × diameter and GPR index

[b] Different correlations were caused by different wavelets used for GPR index extraction

**Table 4** A comparison of root biomass estimation using GPR, showing GPR index, target plant species, antenna center frequency, detection depth, root size, sample size for correlation analysis, and the Pearson correlation coefficient between GPR index and actual root biomass. The definition of each GPR index is shown in Fig. 6

| GPR Index | Species | Antenna center frequency (MHz) | Detection depth (cm) | Root diameter (cm) | Sample size (n) | Correlation coefficient ($r$) | Reference[†] |
|---|---|---|---|---|---|---|---|
| Areas within threshold range | *Pinus taeda* | 1500 | <40 | >0.5 | 64 (16)[a] | 0.34 (0.55)[a] | Butnor et al. 2001 |
| Reflector tally | *P. taeda* | 1500 | <40 | >0.5 | 64 (16)[a] | 0.36 (0.49)[a] | Butnor et al. 2001 |
| Pixels within threshold range | *P. taeda* | 1500 | <30 | >0.5 | 60 | 0.86 | Butnor et al. 2003 |
| | *P. taeda, P. elliottii* | 1500 | - | - | 60 (4)[a] | 0.17 (0.96)[a] | Butnor et al. 2005 |
| | *P. taeda* | 1500 | - | - | 63 (9)[a] | 0.45 (0.77)[a] | Butnor et al. 2005[c] |
| | *P. taeda* | 1500 | - | - | 40 (16)[a] | 0.78 (0.80)[a] | Butnor et al. 2005[c] |
| | *Quercus sp.* | 1500 | - | >0.5 | 30 | 0.88 | Stover et al. 2007 |
| | *P. taeda,* | 1500 | - | - | 40 | 0.51, 0.80[b] | Butnor et al. 2008 |
| | *Q. sp.* | 1500 | - | - | 40 | 0.84, 0.82[b] | Butnor et al. 2008 |
| | *P. taeda* | 1500 | - | - | 84 | 0.89 | Samuelson et al. 2008 |
| Time interval ($\Delta T$) | *Ulmus pumila* | 2000 | <80 | >0.5 | 30 | 0.89 | Cui et al. 2011 |

[†] Except Cui et al. 2011, the rest studies were completed in field conditions

[a] Values listed before parenthesis are sample size numbers and corresponding correlation coefficients for correlation analysis using all soil core coarse root biomass values and GPR indexes; values in parenthesis correspond to correlation analysis using averaged coarse root biomass and GPR indexes in each subplot (or block)

[b] The first values correspond to coefficients between live coarse root biomass and GPR index, and the second values correspond to coefficients between combined live and dead coarse root biomass and GPR index

[c] Different values were obtained from two field experiments in the same location but different sampling time (the upper one in 2003, and the other in 2005)

from reflected signals (including amplitude of reflected wave, high amplitude area, and time interval between zero crossings) (Fig. 6). Among these indexes, reflector tally can be directly counted from processed GPR images without the application of migration and *Hilbert* transformation, but this method was only used in the study of Butnor et al. (2001) where its estimation accuracy was low (Table 4). The other indexes cannot be directly obtained from GPR radargrams. Several signal processing and image converting steps are required before index extraction. Areas (pixels) within threshold range and mean pixel intensity (average intensity of each reflector) need to be extracted from gray scale images converted from processed GPR radargrams. Reflection waveform indexes are extracted from reflected waves of the trace that passes through the center of each root.

Besides different extraction sources (GPR radargrams or reflected waves), GPR indexes can also be separated into signal strength related indexes (including areas or pixels within threshold range, mean pixel density, amplitude of maximum reflected wave, high amplitude area) and time interval indexes. Using signal strength related indexes for root measurement is based on the assumption that root diameter and biomass are positively correlated with reflection strength. Similarly, time intervals between zero crossings of reflected waves are considered to be positively related to root cross section geometry. Because reflections occur at the interfaces of different medium, the continuous two wavelets reflected by target root are produced by the top and bottom of root-soil interfaces. This means that for larger roots, both the root-soil interfaces can be defined from the composite reflection trace. Thus, the time between GPR wave reaching the root top and the bottom is relevant to root diameter (Cui et al. 2011).

4) *Model fitting*: After GPR index extraction, regression models linking GPR signals and actual root measurements can be built. In most studies, simple linear regression models were

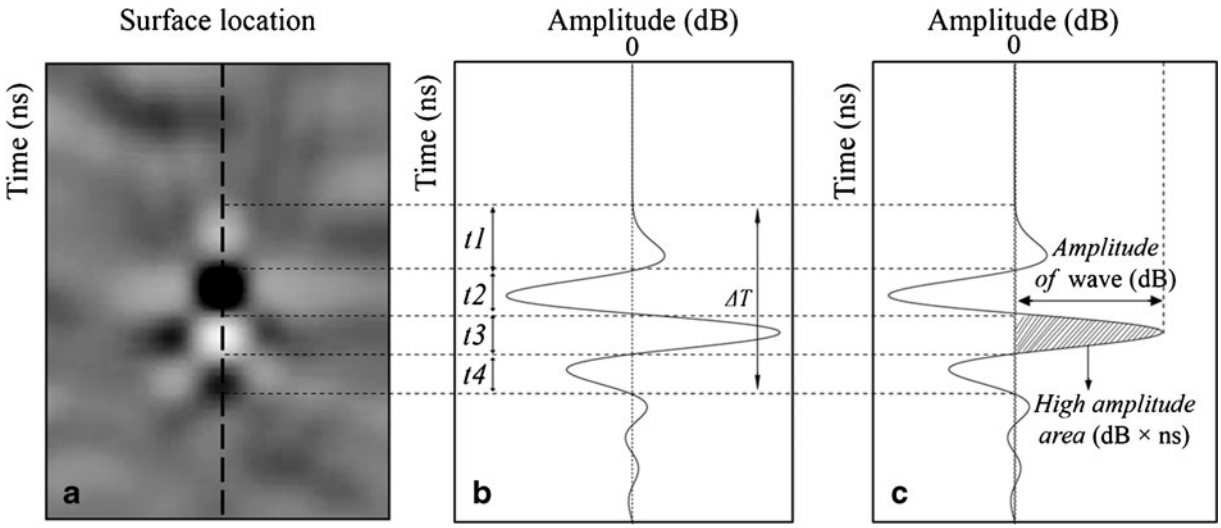


**Fig. 6** Schematic illustration of GPR indexes extraction: **a** A processed 2 GHz GPR radargram showing a root reflector (data from Cui et al. 2011); after being converted to 8-bite gray scale image, the values or pixels within threshold range can be obtained from image analysis software based on the intensity of each pixel (see Fig. 3e); **b** and **c** are the trace passing through the center of the root as indicated by the vertical dashed line in (**a**). **b** shows different time indexes *t1* ~ *t4* and $\Delta T$ that can be determined from the trace as the time interval between zero crossings of the waveform, and **c** shows amplitude of the reflected wave and the high amplitude area extracted from the same trace

used for establishing the relationship between GPR indexes and root parameters. Only Barton and Montagu (2004) and Butnor et al. (2005) applied multiple linear regression model and simple non-linear regression model to quantify the correlations, respectively.

In the following, specific root related parameter estimations based on GPR are summarized.

*Coarse root diameter estimation*

Studies that focused on coarse root diameter estimation are summarized in Table 3. These studies were carried out under controlled conditions in which coarse root samples were reburied into sandy soils at known depth after their diameters were measured. Different GPR systems with antennas of center frequency from 500 MHz to 2,000 MHz were used. In studies conducted by Barton and Montagu (2004) and Cui et al. (2011), coarse root diameters were rather accurately calculated from GPR index, with root mean square error (*RMSE*) of the regression model being 5.60 mm and 3.53 mm, respectively. Six GPR indexes have been designed and used for coarse root diameter, increasing the feasibility of root diameter measurements by GPR (Table 3).

The estimation accuracy of each GPR index is, however, site specific. Many factors (e.g., antenna frequency, soil properties, experimental condition, plant species, sample depth, signal filter process, and others) impact the detection and quantification of roots using GPR (Dannoura et al. 2008; Hirano et al. 2009). Even the same index could produce conflicting results from different studies. For example, Barton and Montagu (2004) reported that the same signal strength indexes successfully used in Butnor et al. (2001) and Butnor et al. (2003) for root diameter estimation were poorly correlated with root size in their study. Dannoura et al. (2008) and Hirano et al. (2009) failed to obtain high estimation accuracy using the time interval index reported by Barton and Montagu (2004). Thus, it is hard to determine which GPR index is more appropriate for coarse root diameter evaluation as compared to other indexes.

Both signal strength indexes and time interval indexes all have their own advantages and flaws for root diameter estimation. For signal strength GPR indexes, which are affected by root size and root depth together, the reflected signal strength decreases at a rate proportional to the fourth power of the penetrating depth due to the absorption and dispersion of EM beams by soils (Barton and Montagu 2004; Cox et al. 2005). Hence,

accurate root diameter estimation cannot be accomplished from only signal strength indexes without considering root depth, especially when root samples are buried at different depths. This can explain why the combined effect of depth and diameter resulted in a stronger correlation ($r$=−0.63) with signal strength index than the relationship between only diameter and reflection strength ($r$=−0.52) in the study of Cox et al. (2005). In addition, the range of threshold value (used for extracting areas/pixels within threshold range) is arbitrarily determined, and thus was different among the cited studies. It is uncertain how variations in threshold range influence the parameters performance on root diameter. Furthermore, the correlation between signal strength and root size is statistical or empirical. The physical mechanism explaining the positive correlation between root size and signal strength is still unclear.

The intervals between successive zero crossings of the reflected waveform where the amplitude of GPR wave is zero are extracted as time interval indexes (Fig. 6b). The most remarkable advantage of time interval indexes is that these indexes only depend on root size regardless of depth (Barton and Montagu 2004; Cui et al. 2011). The main drawback of time interval index is that the relationship between indexes and root size will break down when the orientations of roots are unknown or roots grows in clumps resulting in complex reflectors on GPR radargrams (Barton and Montagu 2004; Butnor et al. 2008). Moreover, the performance of time interval index is closely related to the wavelet from which the indexes are extracted. Barton and Montagu (2004) found that only the time intervals of the first three waves (*t1*, *t2*, *t3* in Fig. 6b) were correlated with root diameter. Dannoura et al. (2008) found that even the time intervals of the first positive wave (*t1* in Fig. 6b) and those of the first negative wave (*t2* in Fig. 6b) produced different correlation coefficients with root size ($r$=0.50 and 0.77, respectively). Nevertheless, it is hard to determine the first wavelet reflected from the targets on GPR traces. Sometimes the waveforms fail to cross the zero line (where wave amplitude is equal to zero) (Barton and Montagu 2004). These limitations would also have impact on the precise extraction of time interval $\Delta T$ used in the study of Cui et al. (2011) (Fig. 6b). To overcome the blurry definition of time interval index, Hirano et al. (2009) used time interval of the maximum reflected wave for root diameter estimation. However, only weak correlation was found between this index and actual root diameter (Table 3).

It should be noted that the GPR-based coarse root diameter estimation studies were all completed in controlled conditions (i.e., straight coarse roots were buried parallel in homogeneous sands with large intervals, and GPR scanning transects were perpendicular to the long axis of the roots), which is far from realistic root distribution in the field. In addition, the results of GPR-based coarse root diameter estimation studies were based on limited sample size (Table 3). Given the complex root distribution patterns in field conditions, using GPR for in situ coarse root diameter estimation still needs considerable improvements.

### *Coarse root biomass estimation*

Coarse root biomass estimation is important for understanding carbon storage and recycling in ecosystems (Stover et al. 2007). Table 4 summarizes the studies on root biomass estimated using GPR. Butnor and colleagues have completed most of these studies. Their research focused on live coarse root biomass estimation of loblolly pine (*Pinus taeda*) under field conditions. Butnor et al. (2001) first found coarse root biomass could be estimated from areas within threshold range and reflector tally counts extracted from GPR images, although their correlations were often exceedingly low. In this study, a total of 64 radar transects were set in 16 subplots. For each of the 64 radar transects, GPR index accounted for approximately one third of the variation in coarse root biomass. The composite of all transects in a subplot improved the correlation between GPR index and coarse root biomass (Table 4). Butnor et al. (2003) further developed a rapid method to estimate coarse root biomass by combining GPR with soil cores on a subset of plots. Importantly, they demonstrated that, with the aid of advanced digital signal processing of GPR data, the accuracy of coarse root biomass estimation could be considerably improved. They also found that the reflection strength suffered from more serious attenuation in fertilized soils. Butnor et al. (2005) applied GPR for coarse root biomass estimation in wet sandy soils. They showed that moisture increased signal attenuation. They also found that it was impossible to separate live roots from buried organic debris, and that thick layers of leaf litter would degrade the ability of GPR for root measurement. In

this study, a non-linear model was first used to quantify the correlation between coarse root biomass and GPR indexes. Similar to Butnor et al. (2001), this study revealed that the correlation between average values of GPR index and coarse root mass in each subplot was significantly stronger than the correlation between GPR index and coarse root biomass from individual root cores (Table 4). Adopting the same GPR data processing and index extraction protocol, Stover et al. (2007), Butnor et al. (2008), and Samuelson et al. (2008) successfully estimated root biomass using pixels within threshold range from GPR images. In these subsequent studies, a standard GPR-based coarse root biomass estimation protocol (especially for GPR data post-processing) was established. Another improvement is that for total belowground biomass estimation, taproot plus adjacent coarse root biomass within 1 $m^2$ area was calculated from aboveground biomass and combined with GPR-based lateral coarse root biomass outside the 1 $m^2$ area (Samuelson et al. 2008). Considering the limitation of GPR for taproot detection, this combined coarse root biomass estimation approach improves the accuracy of GPR-based total belowground biomass assessment. In addition, Butnor et al. (2008) found that the correlation between live coarse root biomass and GPR index would be less desirable than the correlation between combined live and dead coarse root biomass and GPR index (Table 4).

It is noteworthy that all of the above studies failed to estimate coarse root biomass at certain depth. These studies built correlations between total coarse root biomass measured from soil core data and the GPR indexes estimated from corresponding GPR images. Such a limitation might be caused by the use of signal strength indexes, which decrease with penetrating depth, for coarse root biomass estimation without applying signal gain. Furthermore, these studies attempted to evaluate coarse root dry weight from GPR signal strength indexes that were highly related to root water content (Dannoura et al. 2008; Hirano et al. 2009). Because GPR signal strength indexes are a function of root dry weights and their water contents together, low water contents would result in underestimating root biomass. Thus, Hirano et al. (2009) concluded that accurate coarse root biomass could not be estimated using single frequency of GPR.

Different from the above studies, Cui et al. (2011) used a novel time interval index ($\Delta T$) for *Ulmus pumila* coarse root fresh biomass estimation using a 2,000 MHz antenna in dry sandy soils with separated root samples reburied at known depth intervals. By assuming the shape of roots to be cylindrical, they developed a method to estimate root fresh biomass based on root diameter and density. Root diameter was evaluated from $\Delta T$ that was correlated with root geometry regardless of root depth. For *U. pumila*, root density had no clear trend in variation and changes little as diameter increases, when root diameter was greater than 0.5 cm. The average root matter density was measured by collecting a small number of root samples. The indirect estimation method proved the accuracy of coarse root fresh biomass estimation ($r$= 0.92). Cui et al. (2011) also estimated root fresh biomass from $\Delta T$. Although the direct estimation accuracy was lower than the indirect method, a significant correlation was found between $\Delta T$ and root fresh biomass ($r$=0.89). Using time interval index for root biomass estimation could avoid the impact from root depth and root water content. Because the root shape is complex and root density patterns probably vary among species, and it is unclear whether such an indirect method is feasible for root dry weight estimation in field conditions, more studies are required to further test and improve this method.

In summary, GPR-based coarse root biomass assessment has been conducted in the field with reasonable estimation accuracy. Based on the past studies, the best correlation between GPR index and coarse root biomass can be obtained using total root biomass (i.e., undifferentiated by root size class, root depth, living root, and dead root). Future studies should consider the impacts of root water content on GPR-based coarse root biomass estimation and the limitation of GPR for taproot biomass estimation.

## Limiting factors of GPR-based coarse root detection and quantification

As a nondestructive detection instrument, GPR shows some promises for coarse root detection and quantification, but successful application has been site-specific (Butnor et al. 2003). Therefore, it is crucial to clarify what factors can interfere with the reliable investigation of coarse roots by GPR.

Field soil conditions have dramatic impacts on the practicality of coarse root detection and quantification

by GPR. Generally, GPR is most useful in low-electrical-loss materials (Jol 2009). Butnor et al. (2001) found that GPR resolution was best in dry sandy soils but seriously degraded in soils with high water and/or clay contents. Butnor et al. (2005) found that wet soils weakened the correlation between root biomass and GPR index and that thick litter layer on the soil surface degraded the ability of GPR to delineate roots. From GPR theory, soil relative dielectric permittivity ($\varepsilon_r$) and electrical conductivity ($\sigma$) are the most important factors that control the propagation and reflection of GPR signal in the ground (Conyers 2004). The contrast of $\varepsilon_r$ between roots and soils determines the amplitude of reflection signals and $\sigma$ determines the amount of energy that will be attenuated in the soil. For dry sandy soils, low $\varepsilon_r$ (which is usually between 3 and 5) and $\sigma$ values ensure the necessary reflection strength from root reflectors and sufficient penetration depth for GPR pulse. However, even if a small amount of water is added to the soil, the $\varepsilon_r$ of soil will increase dramatically because of the much higher $\varepsilon_r$ value of water (80 ~ 88) (Conyers 2004). Increases in soil moisture decrease the electromagnetic gradient between roots and soils. Therefore, the reflected signals are weakened, making the delineation of roots more difficult under wet conditions (Butnor et al. 2001). In addition, as bipolar molecules, water molecules will rotate and become aligned within an imposed EM field. This rotation will cause GPR energy to be converted to mechanical energy, increasing energy attenuation in the ground (Conyers 2004). The $\sigma$ of soils will increase with increase in water, clay, and soluble salt contents. The more electrically conductive a soil is, the larger amount of energy will be attenuated at a shallower depth. Other buried objects and organic debris in the soil could further limit the ability of GPR to detect roots. Although some belowground objects (e.g., stones, water-filled pipes, cables, and others) can be discriminated from roots (Hruška et al. 1999; Stokes et al. 2002), there are no apparent differences in signals between roots and some buried objects (e.g., dead roots, empty PVC tubes, old pipes, and pebbles) (Butnor et al. 2005; Cox et al. 2005; Zenone et al. 2008; Leucci 2010).

Besides soil water content, root water content is also a key factor in root GPR detection (Hirano et al. 2009). Before Dannoura et al. (2008), most studies emphasized the impact of soil water content on the detection of roots using GPR. Dannoura et al. (2008) found that the gradient in water content between root samples and soils was important to precise root delineation. Hirano et al. (2009) confirmed that dried roots (volumetric water content <20 %) could not be detected by GPR. But few studies have been done to investigate root $\varepsilon_r$ (Hirano et al. 2009). As far as we can tell, no empirical model has been developed to describe the numerical relationship between root $\varepsilon_r$ and its water content. By assuming that a root consists of three components—air, solid solution (composed of wood cellular material and bound water), and free water, a dielectric mixing model for woody biomass (Paz et al. 2011) can be applied:

$$\varepsilon_{rm}^{\beta} = \theta_{fw} \times \varepsilon_{rfw}^{\beta} + \theta \times \varepsilon_{ra}^{\beta} + \theta_s \times \varepsilon_{rs}^{\beta}, \quad (7)$$

where $\varepsilon_r$ is the relative dielectric permittivity, $\theta$ is the volumetric content, and subscript $m$ stands for root mixture, $fw$ for free water, $a$ for air, and $s$ for solid solution, and $\beta$ is the geometric factor compensating for the shape of components and their orientation. The values of $\varepsilon_{rfw}$, $\varepsilon_{ra}$, and $\varepsilon_{rs}$ are 80, 1, and 10, respectively (Paz et al. 2011). From Eq. 7, it is clear that root $\varepsilon_r$ will increase with root moisture content. Al Hagrey (2007) showed that $\varepsilon_r$ of dry wood cellulose is 4.5, while that of wet wood cellulose is 22. Because the reflection power of root is determined by $\varepsilon_r$ contrast between roots and soils, the signal strength of root reflector is closely linked to root water content. Thus, root water content will further influence root biomass estimation from signal strength indexes. Hirano et al. (2009) reported that signal strength indexes from smaller roots with higher water content were higher than those from larger roots with lower water content (e.g., the amplitude of reflected wave and amplitude area extracted from a root with a diameter of 39 mm and a volumetric water content of 48 % were 61 dB and 30 dB × ns, respectively; those from a root with diameter of 46 mm and a volumetric water content of 5 % were only 15 dB and 8 dB × ns, respectively. See Table 1 in Hirano et al. 2009). Therefore, accurate coarse root quantification cannot be accomplished without considering the impact of root water content.

The center frequency of GPR antenna influences the depth of penetration and the detection resolution by GPR (Hruška et al. 1999; Butnor et al. 2001; Barton and Montagu 2004). The maximum effective depth of penetration and resolution of various

frequencies on the detection of roots by GPR have been investigated (Table 1). In general, low-frequency GPR waves can penetrate deeper, but are capable of resolving only larger features. In contrast, high-frequency GPR waves have a higher resolution, but shallower penetration depths. In principle, the cross-sectional area of the target to be delineated should approximate the size of footprint area of the GPR wave (Conyers 2004). The lower the antenna frequency, the longer wavelength and the larger footprint will be produced (Eq. 5). Thus, resolution is positively correlated with antenna frequency. Unfortunately, GPR wave energy attenuation is increased with antenna frequency (Neto and de Medeiros 2006). Therefore, a trade-off exists between penetration depth and resolution (Fig. 7). There are no fixed rules for choosing the optimum frequency in a given survey, but the antenna center frequency should be computed to ensure the propagated wavelength in a medium is smaller than one half the size of the smallest target (Daniels et al. 2004).

Apart from the physical properties of roots, root positions (depth of roots and the intervals between neighboring roots) also influence root detection using GPR. The deeper the target roots is in the ground, the greater the dissipation of the transmission beam, and the greater the energy attenuation. As mentioned above, a compromise must be made between detection depth and resolution, which implies that it is not possible to obtain detection accuracy for deeper targets. In other words, small roots buried deeply in the soil cannot be detected by GPR, no matter what antenna frequency is used. Stokes et al. (2002) reported that GPR has limited ability to reveal crossing-over patterns of roots and branches. Hirano et al. (2009) found that individual *Cryptomeria japonica* roots with intervals less than 20 cm, both horizontally and vertically (which was common for *C. japonica* roots in the field), could not be distinguished from each other and were often considered as one root.

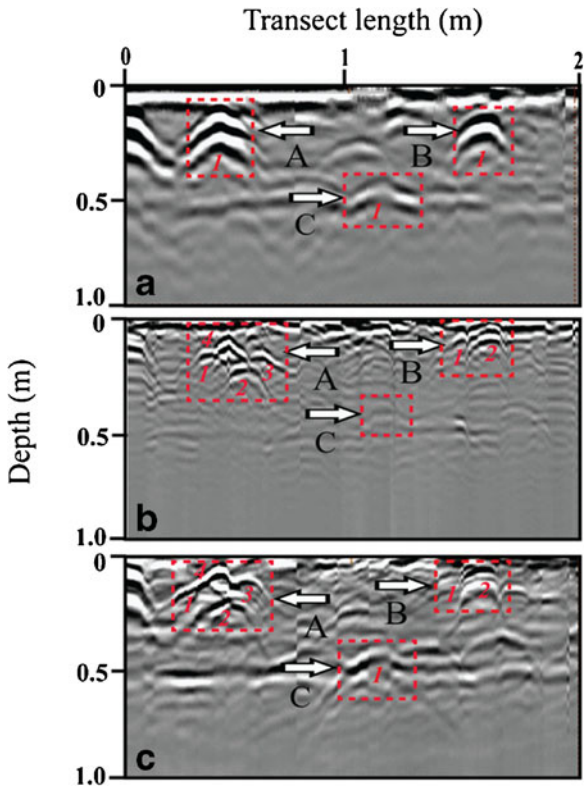


**Fig. 7** Impacts of antenna frequency on GPR radargrams collected from a shrub (*Salix psammophila*) in a sandy area in the Inner Mongolia, China: **a** Raw data obtained from an IDS GPR system with 900 MHz antenna; **b** Raw data obtained with 2,000 MHz antenna; **c** Raw data obtained at the same time with a 900 MHz antenna as transmitting antenna and a 2,000 MHz antenna as receiving antenna. Arrows A and B on each radargram indicate root reflections (i.e., the hyperbolic shaped signals within the dashed square) that were distinguishable in both (**b**) and (**c**) scenarios with different numbers representing each root reflector, but failed to be distinguished in the (**a**) scenario, implying a higher detection resolution in (**b**) and (**c**). Arrow C on each radargram indicates a root buried at 0.5 m depth that were detected in both (**a**) and (**c**) scenarios, but not in (**b**) scenario, implying a deeper penetration range in (**a**) and (**c**). The scale used for plotting the data is identical for each subfigure

## Future outlooks

Since GPR technique was first used to map root system more than 10 years ago, various new applications have been introduced and improved, as reviewed in this paper. In this section, we offer some future outlooks and potential improvements for further enhancement of GPR application in coarse root detection and quantification.

1) *Applying advanced GPR system (*e.g.*, GPR system with multi-frequency antenna and antenna array) and improving in situ data collection protocol.* Confined by the GPR theory, a compromise must be made between improved detection resolution with higher antenna frequency and increased penetration depth with lower antenna frequency (Table 1), which indicates that coarse

roots located deeply in the soil may not be detected well by GPR. However, a whole range of penetration depths and resolutions of GPR may be realized by applying multi-frequency antenna and antenna array, as illustrated in Fig. 7. Several antennae with the same frequency may be used to obtain GPR scans simultaneously, or separate transmitter and receiver antennae operating at different frequencies may be combined into one single antenna array unit. The ability to freely choose any transmitter/receiver combination within the array can integrate the detection depth with reasonable resolution, making the detection of deeply buried coarse roots possible (Fig. 7).

In most GPR-based coarse root in situ investigations (except Zenone et al. 2008), root areas were scanned by GPR in a rectilinear grid. If the direction of root growth extension is parallel to the survey grid, an elongate reflection is generated from a root instead of a hyperbolic reflection. Considering lateral coarse roots are radiating outward from tap root, concentric circle grids allow a quasi-perpendicular intersection with most of the roots (Fig. 8). The application of advanced GPR system and data collection protocol will further enhance GPR-based coarse root detection and quantification.

2) *Optimizing specialized root GPR data processing routines and developing algorithms for automatic root reflector identification and 3D structure*

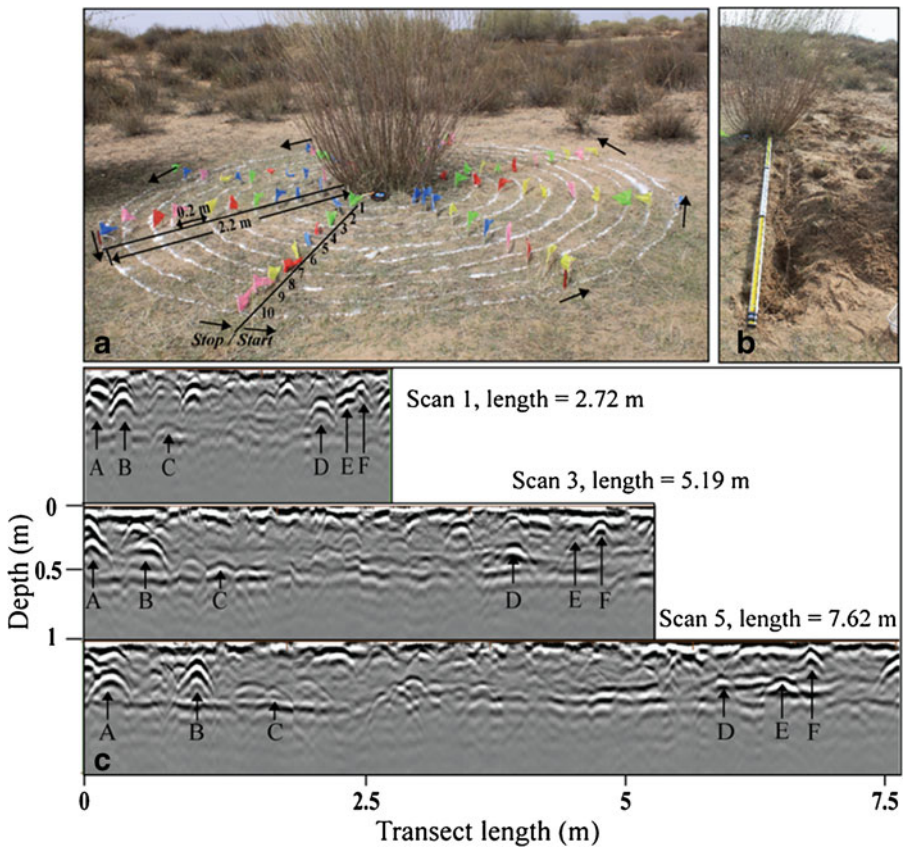


**Fig. 8** Concentric transects used to detect roots by GPR in a sandy area in Inner Mongolia, China: **a** An in situ photograph showing the setting of centric transects used for *Salix psammophila* root detection. Ten circular transects were set around the plant, with 0.2 m interval between neighboring transects. The radius of each transect varied from 0.4 to 2.2 m. Color flags were used for radargram spatial calibration; **b** A shallow root was excavated in situ for ground truthing, which extended between the starting and ending points of the transect (> 3 m long); **c** Corresponding GPR radargrams of scan 1, 3, and 5, respectively, that were generated by an IDS GPR system with 900 MHz antenna frequency. The hyperbolic shaped reflections represent the root reflectors. Same letters on different GPR radargrams indicate the examples of reflections from the same roots. B indicates the GPR signal from the root shown in (**b**). The scale used for plotting the data is identical for each subfigure

*reconstruction*. Although a general root GPR data processing protocol has been determined (e.g., the protocol used in Stover et al. 2007), specific data post-processing steps and software were different among studies, thus limiting the potential of comparison between studies. In addition, specialized root GPR data analysis software with the ability to automatically distinguish root reflectors and link roots between neighboring radargrams is needed to improve the potential of using GPR for coarse root 3D structure reconstruction.

3) *Developing forward simulation models for root GPR reflections synthesis*. Forward simulation is a common method used for imitating the response features of interesting reflectors on simulated radargrams and defining GPR potentials and ambiguities. For those controlled GPR-based coarse root quantification studies, only a few root samples with known parameters (i.e., diameter and water content) were buried at certain depth in nearly homogeneous sandy soil. This type of study can be complemented by forward simulations. Generally, the major input parameters of a GPR simulator (e.g., GprMax by Giannopoulos 2005) include those associated with GPR system settings, the geometries of simulation scenarios, and the EM properties of involved media. These parameters can be directly determined based on the experiment design or calculated from root and soil status. Without considering the limitation of sample size, forward simulation can draw more convincing conclusions with physical mechanisms and predictive capacity.
4) *Developing physical models for coarse root parameters estimation using GPR*. The current estimations are based on statistical relationships between root-related parameters (diameter and biomass) and various indexes extracted from GPR data. The physical mechanisms behind these relationships are still unclear. A possible conceptual model linking GPR indexes and root-related parameters may be expressed as:

$$I = f(f', \varepsilon_s, \sigma_s, \varepsilon_r, \sigma_r, d_1, d_2), \quad (8)$$

where $I$ is the value of indexes extracted from GPR data, $f'$ is the antenna frequency, $\varepsilon$ is the average relative dielectric permittivity, $\sigma$ is average electrical conductivity, $d_1$ is root diameter, $d_2$ is root density, with subscripts $s$ standing for soils and $r$ for roots. These seven independent variables including the information about GPR system, soil EM properties, root EM properties, root geometry and biomass, are the most influential factors for root radar reflection characteristics. The physical model that relates indexes from GPR data with actual root parameters would enhance the estimation accuracy of root diameter and biomass and improve the overall interpretation of root GPR images.

5) *Integration of complementary non-invasive techniques*. In near-surface geophysics, more and more emphasis is placed on the combination (and inversion) of complementary techniques used to detect the same target. Besides GPR, electrical resistivity tomography (ERT) and seismic method have also been applied for root investigations (e.g., Amato et al. 2008; Zenone et al. 2008; Leucci 2010). Currently, these geophysical methods are shown as useful for coarse root detection (al Hagrey 2007; Leucci 2010). Each technique has its own advantage and disadvantage for coarse root investigation (see Table 3 in al Hagrey 2007). However, significant efforts remain needed to determine how best to combine the results from different techniques and integrate the advantage of each technique.

## Summary and Conclusions

Coarse roots play crucial roles in both plant growth and ecosystem services. Root system architecture and root-related parameters (including root diameter and biomass) are fundamental to root functions. As a non-invasive method, GPR has been proved to be a valuable technique for detecting coarse roots in low moisture and electrically-resistive soils. However, the detection and quantification of coarse roots using GPR is still in its infancy and not all roots or soil conditions are suited for this technology. Most GPR root detection studies have been conducted under controlled experimental conditions or within plantations. The primary detection targets were tree root systems. Presently, only the coarse roots that grow laterally and distribute in shallow subsoils (generally <1 m depth) and with enough moisture contrast with the surrounding

soils can be detected and measured by GPR. The biomass of root clusters can be estimated from GPR images, but the identification of each closely-spaced, individual root cannot be accomplished by GPR. Resolution and observation depth of root GPR images achieve the best quality in dry, sandy soils, where a sufficient contrast of dielectric permittivity is provided between roots and their surrounding soils and radar energy is not rapidly attenuated. In contrast, soils with high water content, clay content, and/or soluble salt content decrease the contrast and increase soil electrical conductivity, thus seriously degrading GPR signal and the potential for root detection using GPR. In addition, thick layers of leaf litter on soil surface impact the resolution and observation depth. Hence, sandy soils with low concentrations of organic matters and soluble salts are the most suitable condition for coarse root investigation by GPR. Antenna frequency and root moisture content are other important factors that influence GPR detection of roots. A combination of high antenna frequency with increased resolution and low antenna frequency with deeper observation depth is recommended. Overall, successful GPR-based coarse root investigation is site specific, and only under suitable experiment conditions can reliable measurements be accomplished.

Up to now, coarse root detection, 2D/3D coarse root zone mapping, single coarse root 3D structure reconstruction, and coarse root biomass and diameter estimation can be accomplished using GPR given suitable site conditions and plant species. However, it is difficult to reconstruct coarse root system 3D architecture using GPR at the present. In addition, the current GPR-based coarse root diameter estimation remains challenging under field conditions. Therefore, using GPR for coarse root biomass estimation is the most appropriate direction of applying GPR for field root investigation, especially after taking into account the impact of root moisture content on GPR-based coarse root biomass estimation. Considerable efforts remain needed to achieve improvements in GPR system design, data processing software, field data collection routines, and root-related parameters estimation methods. Developing numerical models for root GPR radargrams may help recognize the linkage between root properties and root GPR signals, thus benefiting the differentiation of root reflections on GPR radargram.

Since GPR technique was first used to map root system more than 10 years ago, various new applications have been introduced and improved, as reviewed in this paper. Based on the experience accumulated so far, we have offered some potential improvements for further enhancement of GPR application in coarse root detection and quantification. In addition, some possible future applications of root detection using GPR include: 1) root development observation over time using repeated GPR scans, tracing root turnover dynamics and root water content variations at different temporal scales or among different environment settings; and 2) root system 3D architecture reconstruction that can provide detailed information of root distribution density at various soil depths, the branching patterns or topology of lateral roots, and the total volume of the root zone.

**Acknowledgments** This study was supported by the National Natural Science Foundation of China (Grant No. 41001239), the research fund of Jin Chen from the Ph.D. Programs Foundation of the Ministry of Education of China, and the State Key Laboratory of Earth Surface Processes and Resource Ecology at Beijing Normal University. The authors also thank three anonymous reviewers for their detailed and valuable comments.

## References

al Hagrey SA (2007) Geophysical imaging of root-zone, trunk, and moisture heterogeneity. J Exp Bot 58:839–854. doi:10.1093/jxb/erl237

Amato M, Basso B, Celano G, Bitella G, Morelli G, Rossi R (2008) In situ detection of tree root distribution and biomass by multi-electrode resistivity imaging. Tree Physiol 28:1441–1448. doi:10.1093/treephs/28.10.1441

Annan AP, Cosway SW (1994) GPR frequency selection. In: Proceedings of the 5th International Conference on Ground Penetrating Radar, Waterloo Center for Groundwater Research, Waterloo Canada, pp 747–760

Barton CVM, Montagu KD (2004) Detection of tree roots and determination of root diameters by ground penetrating radar under optimal conditions. Tree Physiol 24:1323–1331. doi:10.1093 /treephs/24.12.1323

Bassuk N, Grabosky J, Mucciardi A, Raffel G (2011) Ground-penetrating Radar Accurately Locates Tree Roots in Two Soil Media Under Pavement. Arboricult Urban For 37:160–166

Berntson GM, Farnsworth EJ, Bazzaz FA (1995) Allocation, within and between organs, and the dynamics of root length changes in two birch species. Oecologia 101:439–447. doi:10.1007/BF00329422

Brassard BW, Chen HYH, Bergeron Y, Pare D (2011) Coarse root biomass allometric for *Abies balsamea*, *Picea mariana*, *Pinus banksiana*, and *Populus tremuloides* in the boreal forest of Ontario, Canada. Biomass Bioenergy 35:4189–4196. doi:10.1016/j.biombioe.2011.06.045

Brunner I, Godbold DL (2007) Tree roots in a changing world. J Forest Res 12:78–82. doi:10.1007/s10310-006-0261-4

Butnor JR, Doolittle JA, Kress L, Cohen S, Johnsen KH (2001) Use of ground-penetrating radar to study tree roots in the

southeastern United States. Tree Physiol 21:1269–1278. doi:10.1093/treephs/21.17.1269

Butnor JR, Doolittle JA, Johnsen KH, Samuelson L, Stokes T, Kress L (2003) Utility of ground-penetrating radar as a root biomass survey tool in forest systems. Soil Sci Soc Am J 67:1607–1615. doi:10.2136/sssaj2003.1607

Butnor JR, Roth B, Johnsen K (2005) Feasibility of Using Ground-penetrating Radar to Quantify Root Mass in Florida's Intensively Managed Pine Plantation. FBRC Report #38

Butnor JR, Stover DB, Roth BE, Johnsen KH, Day FP, McInnis D (2008) Using Ground-Penetrating Radar to Estimate Tree Root Mass Comparing Results from Two Florida Surveys. In: Allred BJ, Daniels JJ, Ehsani MR (eds) Handbook of Agricultural Geophysics. CRC Press, Boca Raton, pp 375–382

Cammarano F, Piro S (1997) Application of GPR method to locate and reconstruct archeological structures in the S. Cecilia Basilica (Roma, Italy). In 1st Intl. Workshop: Electric, Magnetic and Electromagnetic Methods Applied to Cultural Heritage. Ostuni, Italy. 24 pages

Čermák J, Hruška J, Martinková M, Prax A (2000) Urban tree root systems and their survival near houses analyzed using ground penetrating radar and sap flow techniques. Plant Soil 219:103–116. doi:10.1023/A:1004736310417

Čermák J, Nadezhdina N, Meiresonne L, Ceulemans R (2008) Scots pine root distribution derived from radial sap flow patterns in stems of large leaning trees. Plant Soil 305:61–75. doi:10.1007/s11104-007-9433-z

Conyers LB (2004) Ground-Penetrating Radar for Archaeology. Altamira Press, Walnut Creek

Conyers LB, Goodman D (1997) Ground-penetrating radar: An Introduction for Archaeologist. Altamira Press, Walnut Creek

Cox KD, Scherm H, Serman N (2005) Ground-penetrating radar to detect and quantify residual root fragments following peach orchard clearing. HortTechnology 15:600–607

Cui XH, Chen J, Shen JS, Cao X, Chen XH, Zhu XL (2011) Modeling tree root diameter and biomass by ground-penetrating radar. Sci China Earth Sci 54:711–719. doi:10.1007/s11430-010-4103-z

Daniels DJ (1996) Surface-penetrating radar. The Institute of Electrical Engineers, London

Daniels DJ (2004) Ground penetrating radar, 2nd edn. Institution of Electrical Engineers, London

Danjon F, Reubens B (2008) Assessing and analyzing 3D architecture of woody root systems, a review of methods and applications in tree and soil stability, resource acquisition and allocation. Plant Soil 303:1–34. doi:10.1007/s11104-007-9470-7

Dannoura M, Hirano Y, Igarashi T, Ishii M, Aono K, Yamase K, Kanazawa Y (2008) Detection of *Cryptomeria japonica* roots with ground penetrating radar. Plant Biosyst 142:375–380. doi:10.1080/11263500802150951

Deans JD (1981) Dynamics of Coarse Root Production in a Young Plantation of *Picea sitchensis* 54:139–155. doi:10.1093/forestry/54.2.139

Doolittle JA, Miller WF (1991) Use of ground-penetrating radar in archaeological investigations. In: Behrens CA, Sever TL (eds) Application of Space-Age Technology in Anthropology Conference Proceedings. NASA Science and Technology Laboratory pp 81–94

Giannopoulos A (2005) Modelling ground penetrating radar by GprMax. Constr Build Mater 19:755–762. doi:10.1016/j.conbuildmat.2005.06.007

Hirano Y, Dannoura M, Aono K, Igarashi T, Ishii M, Yamase K, Makita N, Kanazawa Y (2009) Limiting factors in the detection of tree roots using ground-penetrating radar. Plant Soil 319:15–24. doi:10.1007/s11104-008-9845-4

Hruška J, Čermák J, Sustek S (1999) Mapping tree root systems with ground-penetrating radar. Tree Physiol 19:125–130. doi:10:1093/treephs/19.2.125

Jol HM (2009) Ground Penetrating Radar: Theory and Application. Elsevier Science, Oxford

Kalliokoski T, Nygren P, Sievanen R (2008) Coarse root architecture of boreal tree species growing in mixed stands. Silva Fennica 42:189–210

Leucci G (2010) The use of three geophysical methods for 3D images of total root volume of soil in urban environments. Explor Geophys 41:268–278. doi:10.1071/eg09034

Lorenzo H, Perez-Gracia V, Novo A, Armesto J (2010) Forestry applications of ground-penetrating radar. Forest Syst 19:5–17

Miller AT, Allen HL, Maier CA (2006) Quantifying the coarse-root biomass of intensively managed loblolly pine plantations. Can J Forest Res 36:12–22. doi:10.1139/X05-229

Millikin CS, Bledsoe CS (1999) Biomass and distribution of fine and coarse roots from blue oak (*Quercus douglasii*) trees in the northern Sierra Nevada foothills of California. Plant Soil 214:27–38. doi:10.1007/s11104-008-9845-4r

Misra RK, Turnbull CRA, Cromer RN, Gibbons AK, LaSala AV (1998) Below-and above-ground growth of *Eucalyptus nitens* in a young plantation – I. Biomass. Forest Ecol Manag 106:283–293. doi:10.1016/S0378-1127(97)00339-3

Nadezhdina N, Čermák J (2003) Instrumental methods for studies of structure and function of root systems of large trees. J Exp Bot 54:1511–1521. doi:10.1093/jxb/erg154

Neto PX, de Medeiros WE (2006) A practical approach to correct attenuation effects in GPR data. J Appl Geophys 59:140–151. doi:10.1016/j.jappgeo.2005.09.002

Oliveria MRG, van Noordwijk M, Gaze SR, Brouwer G (2000) Auger Sampling, Ingrowth Cores and Pinboard Methods. In: Smit AL, Bengough AG, van Noordwijk M, Pellerin S, van de Geijn SC (eds) Root Methods: A hand book. Springer-Verlad, Berlin, pp 175–210

Oppenheim AV, Schafer RW (1975) Digital signal processing. Prentice Hall, Englewood Cliffs

Papamarinopoulos StP, Papaionnou M, Stefanopoulos P (1997) Explanation of a religious miracle at a Byzantine Church with geophysical methods at South Greece. In 1st Intl. Workshop: Electric, Magnetic and Electromagnetic Methods Applied to Cultural Heritage. Ostuni, Italy. 25pages

Paz A, Thorin E, Topp C (2011) Dielectric mixing models for water content determination in woody biomass. Wood Sci Technol 45:249–259. doi:10.1007/s00226-010-0316-8

Persson HA (2002) Root systems of Arboreal Plants. In: Weisel Y, Eshel A, Kafkafi U (eds) Plant roots: the hidden half, 3rd edn. Marcel Dekker, New York, pp 187–204

Polomski J, Kuhn N (2002) Root Research Methods. In: Weisel Y, Eshel A, Kafkafi U (eds) Plant roots: the hidden half, 3rd edn. Marcel Dekker, New York, pp 295–322

Resh SC, Battaglia M, Worledge D, Ladiges S (2003) Coarse root biomass for eucalypt plantations in Tamsmania, Australia: sources of varation and methods for assessment. Trees 17:389–399. doi:10.1007/s00468-003-0250-6

Reubens B, Poesen J, Danjon F, Geudens G, Muys B (2007a) The role of fine and coarse roots in shallow slope stability and soil erosion control with a focus on root system architecture: a review. Tree Struct Funct 21:385–402. doi:10.1007/s00468-007-0132-4

Reubens B, Windey J, Danjon F et al. (2007b) Root system architecture of woody species important for erosion contol in Tigray, Northern Ethiopia. Proc. 4th Int. Symp. On Dynamics of Physiological Processes in Roots of Woody Plants. 16th-19th September 2007, Bangor, U.K. pp 87

Samuelson LJ, Butnor J, Maier C, Stokes TA, Johnsen K, Kane M (2008) Growth and physiology of loblolly pine in response to long-term resource management: defining growth potential in the southern United States. Can J Forest Res 38:721–732. doi:10.1139/x07-191

Schoor M, Colvin C (2009) Tree root mapping with ground penetrating radar. 11th SAGA Biennial Technical Meeting and Exhibition Swaziland, 16–18 September 2009, pp 371–374

Stokes A, Fourcaud T, Hruška J, Čermák J, Nadezhdina N, Nadyezhdin V, Praus L (2002) An evaluation of different methods to investigate root system architecture of urban trees in situ: 1. Ground-Penetrating Radar. J Arboricult 28:2–10

Stover DB, Day FP, Butnor JR, Drake BG (2007) Effect of elevated Co-2 on coarse-root biomass in Florida scrub detected by ground-penetrating radar. Ecology 88:1328–1334. doi:10.1890/06-0989

Van Noordwijk M, Brouwer G, Meijboom F, Oliveria MRG, Bengough AG (2000) Trench Profile Techniques and Core Break Methods. In: Smit AL, Bengough AG, van Noordwijk M, Pellerin S, van de Geijn SC (eds) Root Methods: A hand book. Springer-Verlad, Berlin, pp 211–234

Wielopolski L, Hendrey G, Daniels J, McGuigan M (2000) Imaging tree root systems in situ. In: Noon DA, Stickley GF, Longstaff D (eds) GPR 2000: Proceedings of the Eighth International Conference on Ground Penetrating Radar, vol 4084. Proceedings of the Society of Photo-Optical Instrumentation Engineers (Spie). pp 642–646. doi:10.1117/12.383538

Zenone T, Morelli G, Teobaldelli M, Fischanger F, Matteucci M, Sordini M, Armani A, Ferre C, Chiti T, Seufert G (2008) Preliminary use of ground-penetrating radar and electrical resistivity tomography to study tree roots in pine forests and poplar plantations. Funct Plant Biol 35:1047–1058. doi:10.1071/fp08062